The estimation of platinum flotation grade from froth image features by using artificial neural networks

by C. Marais* and C. Aldrich*

Transaction Paper

Synopsis

The use of machine vision in the monitoring and control of metallurgical plants has become a very attractive option in the last decade, especially since computing power has increased drastically in the last few years. The use of cameras as a non-intrusive measurement mechanism not only holds the promise of uncomplicated sampling but could provide more consistent monitoring, as well as assistance in decision making and operator and metallurgist training. Although the very first applications of machine vision were in the platinum industry, no automated process control has been developed for platinum group metals (PGMs) as yet. One of the reasons is that to date froth features could not be related to key performance indicators, such as froth grade and recovery.

A series of laboratory experiments was conducted on a laboratory-scale platinum froth flotation cell in an effort to determine the relationship between the platinum grade and a combined set of image features and process conditions. A fractional factorial design of experiments was conducted, investigating 6 process conditions, namely air flow rate (x_1), pulp level (x_2), collector dosage (x_3), activator dosage (x_4), frother dosage (x_5) and depressant dosage (x_6), each at levels. Videos were recorded and analysed to extract 20 texture features from each image.

By using artificial neural networks (ANN), the nonlinear relationship between the image variables and process conditions and the froth flotation grades could be established. Positive results indicate that the addition of image features to process conditions could be used as sufficient input into advanced model based control systems for flotation plants.

Keywords
Flotation, machine vision, image analysis, neural networks.

Background

The implementation of image analysis as an aid in monitoring and control has been investigated extensively due to its non-intrusive nature and other potential benefits, such as more consistent monitoring, higher sampling rate, and shorter duration grade estimates, and therefore quicker operator response, operator and metallurgist training and assistance in decision making. However, comparatively few applications in automated process control of flotation systems have been reported, particularly in the platinum industry. One of the reasons is that to date froth features could not be related to key performance indicators such as froth grade and recovery. The research focus areas have been the use of froth appearance to detect predefined operational states (Moolman *et al.* 1995; Holtham *et al.* 2002; Cipriano *et al.* 1997, 1998; Van Olst *et al.* 2000; Kaartinen *et al.* 2006; Aldrich *et al.* 1997) and the relation between the appearance and operational variables and plant conditions (Aldrich *et al.* 2000; Feng *et al.* 2000; Citir *et al.* 2004; Barbian *et al.* 2007; Banford *et al.* 1998; Aldrich *et al.* 1997). Although these contributions are significant to our understanding of the flotation process, few have been implemented for automated control. In this paper, we have aimed our efforts towards the estimation of froth grade from froth image data and process conditions.

We will briefly discuss the experimental work and feature extraction in the next two sections. Some explanation of the technique used to investigate the relationship between the features and flotation performance will follow. We will end off with conclusions drawn from this study.

Experimental work

A series of batch flotation test was done at the University of Stellenbosch in South Africa on a 4.5 L Barker laboratory flotation cell equipped with a fixed rotor and aerator unit. The ore used was UG2 from Rustenburg provided by Anglo Platinum.

The fractional factorial experimental design was of the form 26-3 i.e. an 1/8th fraction of runs generated by binary combination of six factors measured at two levels as summarized in Table I.

* *Department of Process Engineering, University of Stellenbosch, Matieland, Stellenbosch, South Africa.*

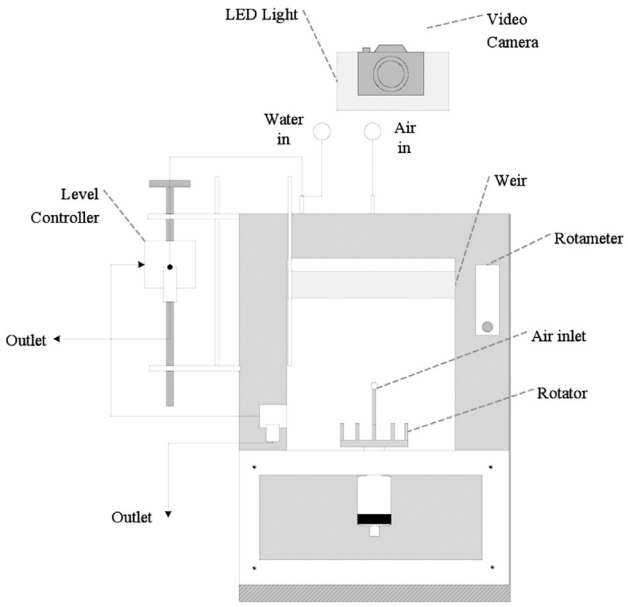

Figure 1—Diagram of the experimental set-up showing the batch flotation cell and camera on top

Table I

Fractional factorial design

Run	x_1	x_2	x_3	x_4	x_5	x_6
1	-	-	+	-	+	-
2	-	+	+	+	-	-
3	-	+	-	-	-	+
4	-	-	-	+	+	+
5	+	-	-	-	-	-
6	+	+	-	+	+	-
7	+	+	+	-	+	+
8	+	-	+	+	-	+

The experiments were conducted in completely random order to avoid biased results. The six variables considered were air flow rate (x_1), pulp level (x_2), collector (x_3), activator (x_4), frother (x_5) and depressant (xx_6). A series of scoping tests were done to find the two levels for the design in order to keep to a mass pull restriction. The mass pull minimum should allow enough froth to be scraped off as a sample and the maximum should not overflow the cell spontaneously. The levels that were used are summarized in Table III.

A representative sample of ore was milled in a 9L rod mill to obtain the desired particle size. A grinding curve was constructed for the particular ore to determine the milling time necessary to obtain the desired particle size. Collector ($CuSO_4$) was added to the mill to allow immediate contacted with the freshly liberated precious metal. The pulp from the mill was then transferred to the batch cell. The rotator was set to a speed in order to maintain a well-mixed pulp. An initial conditioning stage was performed in which the specified amount of collector and activator was added and allowed to condition for 2 minutes, after which the depressant and frother followed suit. The air flow rate, impeller speed and pulp height were then adjusted according to specifications. After a froth build-up time of approximately 30 seconds the first float was sampled, immediately followed by the next.

According to the flotation procedure (Table II), the froth was scraped off every 20 seconds for a specified duration: Float 1 lasted 2 minutes, float 2 was 6 minutes, float 3 was 12 minutes and the last two floats were 10 minutes each. The third float was followed by a second conditioning with different dosage specifications. The sampling of float 4 began immediately thereafter. All the floats, a feed sample and the remaining tails were filtered, dried and analysed for platinum, paladium, copper and nickel.

Video recordings were made of the froth with the use of the Sanyo Xacti, high definition (1280 x 720), waterproof video camera, at a frame rate of 29.976 frames per second (fps). A custom built LED light, consisting of a configuration of six 1W LEDs, provided lighting in such a way as to minimize the interference of ambient light. It was situated approximately 25 cm above the cell.

Image analysis

Image acquisition

Each experimental run generated approximately 85000 images of size 1280 x 720. These images were processed off-line on a standard PC using the Matlab 6.2 image processing toolbox. Matrices with red, green and blue element values representing each pixel for each frame were converted to greyscale for further analysis.

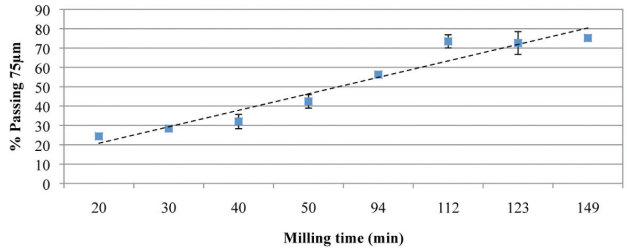

Figure 2—Ore grinding curve

Table II

Laboratory flotation flow sheet (x indicates when reagents are added)

	t (min)	Reagent addition			
		Collector	Activator	Depressant	Frother
Take feed sample					
Condition 1a	2	x	x		
Condition 1b	2		x	x	
Measurements—pH, T(°C)					
Air on (allow 30s froth build-up time)					
Float 1	2	Scrape sample every 20 seconds			
Float 2	6	Scrape sample every 20 seconds			
Float 3	12	Scrape sample every 20 seconds			
Condition 2a	2	x	x		
Condition 2b	2			x	x
Float 4	10	Scrape sample every 20 seconds			
Float 5	10	Scrape sample every 20 seconds			
Measurements—pH, T(°C)					
Tails		Filter and sample			

Table III

Levels of factors used in the experiments

Variable	High (+)	Low (-)
Air flow rate (L/min)	6	4
Impeller speed (rpm)	1100	900
Pulp height (cm below cell lip)	2	3
Particle size (-75μm)	60%	80%
$CuSO_4$ (g/t)	66	54
1st conditioning (g/t)		
SIBX (collector)	88	72
Senkol 65 (activator)	22	18
KU9 (depressant)	55	45
XP 200 (frother)	55	45
2nd conditioning(g/t)		
SIBX (collector)	99	81
Senkol 65 (activator)	0	0
KU9 (depressant)	33	27
XP 200 (frother)	11	9

Feature extraction

A Grey level co-occurrence matrix was created from each matrix of pixel intensities from which four features were extracted: contrast, correlation, energy, and homogeneity.

The spatial grey level dependence matrix (SGLDM) is based on the estimation of the second-order joint conditional probability density functions, $f(i,j,d,a)$, a = 0°, 45°, 90°, 135°. Each function is the probability of going from grey level i to grey level j, given that the intersample spacing is d and the direction is given by angle a. If an image has g grey levels, then the density functions can be represented as $g \times g$ matrices. Each matrix can be computed from a digital image by counting the number of times each pair of grey levels occurs with separation d and in the direction specified by a. It is assumed that the textural information is sufficiently specified by the full set of five spatial grey level dependence matrices. Haralick *et al.* (1973) proposed a set of measures for characterizing these matrices. The features (f_{nm}, n: settings (1–4), m: features (1–5)) are used most often. The fifth feature of the proposed compilation, termed entropy, created some difficulties in further analysis due to the zero variance vectors it produces at settings 3 and 4, and were therefore not included in the feature set. The remaining features are described as follows:

Energy ($f_{n,1}$):

$$E = \sum_i \sum_j \left[f(i,j,d,a) \right]^2 \quad [1]$$

Energy is a measure of the homogeneity of the image. The diagonal and region close to the diagonal represent transitions between similar grey levels. Therefore, for a more homogeneous image the matrix will have a large number of large entries off the diagonal, and hence the energy (E) will be large.

Entropy ($f_{n,2}$):

$$e_{\epsilon} = -\sum_i \sum_j \left[g(i,j,d,a) \cdot \log\left(g(i,j,d,a) \right) \right] \quad [2]$$

The entropy is a measure of the complexity of the image, i.e. a complex image tends to have a higher entropy value than a simple one.

Inertia ($f_{n,3}$):

$$I = \sum_i \sum_j \left[(i-j)^2 f(i,j,d,a) \right] \quad [3]$$

The inertia is a measure of the number of local variations in the image. Therefore an image with a large number of local variations will have a larger value of inertia.

Local homogeneity ($f_{n,4}$):

$$LH = \sum_i \sum_j \left[f(i,j,d,a) / \left(1 - (i+j)\right)^2 \right] \quad [4]$$

Homogeneity is the measure of the tendency of similar grey levels to be neighbours.

Correlation ($f_{n,5}$):

$$COR = \sum_i \sum_j \left[(i-\mu_x)(j-\mu_y) \cdot \left(f(i,j,d,a) / (\sigma_x \sigma_y) \right) \right] \quad [5]$$

Correlation is a measure of the grey level linear dependencies in the image. μ_x and σ_x are the mean and standard deviation of the row sums of the matrix, and μ_y and σ_y are the mean and standard deviation of the column sums.

Each of these features were calculated at five different image settings: default greyscale (s_1), histogram equalized (s_2), contrast enhanced (s_3) and binary (s_4) resulting in a total of 20 image features (see Figure 3).

Histogram equalization improves the contrast of images. The intensity values of the pixels are transformed so that the histogram of the output image closely matches a specified histogram.

Contrast enhancement increases the contrast of the output image by adjusting a grey scale image to a new set of values so that 1% of data is saturated at low and at high intensities of the input image.

Binary images are obtained with the application of a pixel intensity threshold. A global threshold is chosen to minimize interclass variance of black and white pixels (Otsu's method). Pixel values that are smaller than the threshold value will be given the smallest value (black); the opposite is true for larger values.

The representative features for the floats were extracted from the data and the average number of observations per run was approximately 17 400. The grade for each float was assumed to be the same for all the representative images during that sampling duration. The final data-set used for each run was as illustrated in Figure 4.

Incidentally, traditional segmentation techniques, e.g. watershed segmentation, could not be applied successfully to the images due to the froth appearance. From Figure 3 it is evident that the bubbles are very small and therefore not all of them had clearly identifiable reflection points. Furthermore, the bubbles are not heavily loaded therefore a lot of clear windows are visible and in some instances appear darker than the bubble edges. These shortcomings prohibited the identification of markers and subsequent detection of edges.

Relationship between features and froth grade

Artificial neural networks (ANNs) is a nonlinear function mapping technique that has grabbed the attention of many researchers since its appearance. It is effective technique, yet simple to unfold and not computationally expensive.

A multilayer perceptron (MLP) network usually consist of three layers of nodes as illustrated in Figure 5. Each node links to another node with a weighted connection, $w(i,j)$.

$\boldsymbol{X}$ is a set of n-dimensional input vectors:

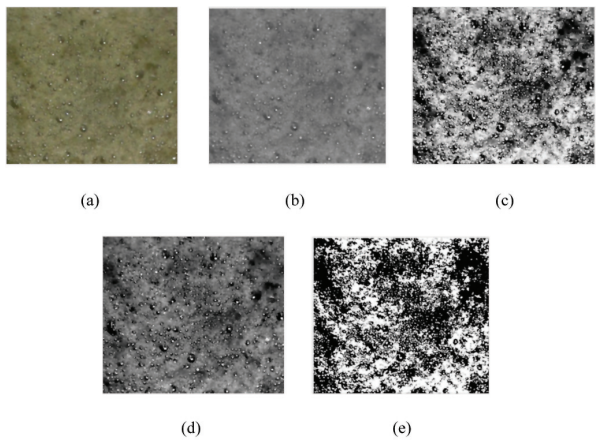

Figure 3—A froth image at the different settings: (a) RGB image, (b) Gray scale/intensity image, (c) histogram equalized image, (d) contrast enhanced image and (e) binary image

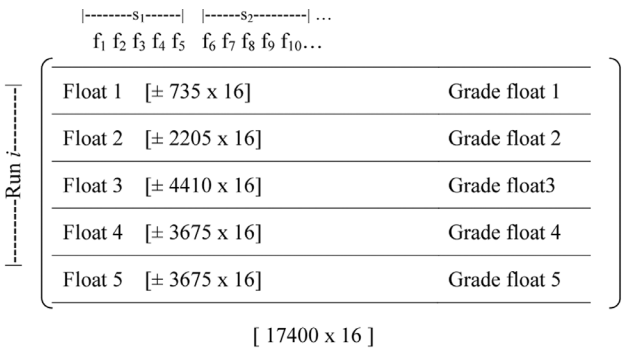

Figure 4—Illustration of the data-set structure for an experimental run

$$\mathbf{X} = \{\boldsymbol{x}_p\}, p = 1,2,3,...P$$
$$\boldsymbol{x} = [x_1, x_2, x_3, ..., x_n] \quad [6]$$

$\boldsymbol{Y}$ is a set of k-dimensional output vectors:

$$\boldsymbol{Y} = \{\boldsymbol{y}_p\}, p = 1,2,3,...P$$
$$\boldsymbol{y} = [y_1, y_2, y_3, ..., y_k] \quad [7]$$

ϕ is a set of m activation functions.

$\mathbf{W^H}$ is the network weight matrix of size $m \times j$ referring to the weights between the input and hidden nodes. $\mathbf{W^O}$ is the network matrix of size $m \times k$ referring to the weights between the hidden and output nodes. The network function for the kth output can therefore be formally expressed as:

$$y_k = \varphi_k\left(\sum_{m=0}^{M} W_{m,k}^{0}\varphi_m\left(\sum_{n=0}^{N} W_{n,m}^{H} X_n\right)\right) \quad [8]$$

The performance of an ANN is measured by the root-mean-square error (RMSE) which is also the function to be minimized. Since this is a minimization problem, general algorithms for unconstrained optimization can be used (Ripley, 2009).

$$RMSE = \sqrt{\frac{\sum_{n=1}^{N} SSE_n}{NK}} \quad [9]$$

N refers to the training vector number (i.e. observation) and SSE_i is the sum-square error of the ith training vector for all K output nodes:

$$SSE_n = \sum_{k=1}^{K}\left(y_{true,k}^{n} - y_{pred,k}^{n}\right)^2 \quad [10]$$

The weight matrices ($\boldsymbol{W^H}$ and $\boldsymbol{W^O}$) are initially randomized. A subset of the input data-set is applied to the network input nodes and the outputs of the hidden and output nodes are calculated. The *SSE* is calculated as in Equation [10] upon which the weight matrices are updated using the optimization framework. The procedure is repeated for the remaining input data-set to calculate the *RMSE* which completes a single iteration. A number of these iterations are necessary to minimize the *RMSE* (Kalyani *et al.* 2008).

The R^2 value was used as indicator of accuracy and is simply the squared value of the correlation coefficient of the predicted and true grade value sets:

$$R^2 = 1 - \frac{\sum_i^n \left(y_{true,i} - y_{pred,i}\right)}{\sum_i^n \left(y_{true,i} - \overline{y_{true}}\right)} \quad [11]$$

Results

The relative assay results from the experimental runs are shown in Figure 6. The data-set consisted of 10 000 observations and it was divided into three sets to be used for training, testing and validation of the model.

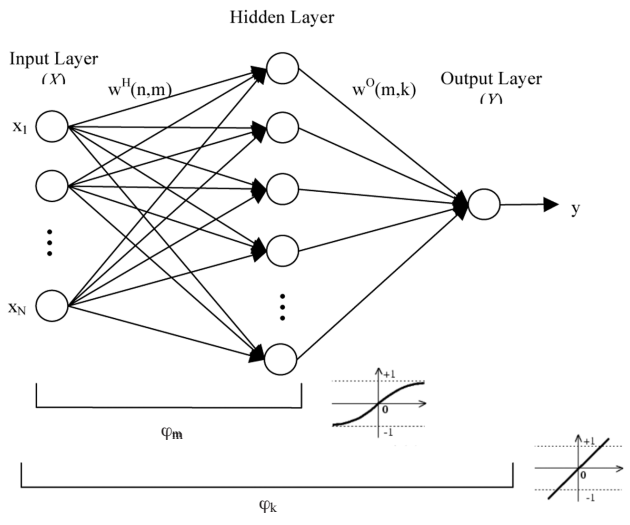

Figure 5—Multilayer perceptron neural network

The testing results show an average R^2 value of 0.943. Each experiment represents a different set of plant conditions and the results in Table IV indicate that, under steady state conditions, a neural network would be able to give reasonable estimates of the grade of the froth.

For the experimental study each neural network input layer had 19 dimensions (N=19), consisting of the 19 texture features (the binary entropy had to be omitted from the data-set due to a standard deviation of 0). A number of possible network architectures were tested for each experiment to determine the appropriate amount of hidden nodes (M) and the activation functions. The error function ($RMSE$) was minimized using the error-back-propagation algorithm using a gradient-descent technique. The best performing networks are summarized in Table IV.

The neural network built on the textural features performed well with an average R^2 value of 0.943 from which it was evident that the grade can be predicted reliably from image information alone.

With a video camera installed on the plant, new image data may be introduced to the model to provide an estimate of the froth grade. However, significant changes in the process conditions would require retraining of the model, as would typically be required on a plant, where process drift and other changes related to process disturbances or changes in equipment would be encountered.

Conclusions

The results show that ANN modelling is an effective way of predicting flotation froth grade. It should, in theory, be relatively easy to implement as an inverse model for control due to the known activation functions and weights, or as the basis for advanced control dependent on a model. These possibilities are being explored for implementation at Anglo Platinum. The additional advantage of low computational expense makes this an ideal technique to consider for potential online application.

References

Aldrich, C., Moolman, D.W., Bunkell, S.-., Harris, M.C., and Theron, D.A. Relationship between surface froth features and process conditions in the batch flotation of a sulphide ore. *Minerals Engineering*, vol. 10, no. 11, 1997a, pp. 1207–1218.

Aldrich, C., Moolman, D.W., Gouws, F.S., and Schmitz, G.P.J. Machine learning strategies for control of flotation plants. *Control Engineering Practice*, vol. 5, no. 2, 1997b, pp. 263–269.

Aldrich, C., Schmitz, G.P.J., and Gouws, F.S. Development of fuzzy rule-based systems for industrial flotation plants by use of inductive techniques and genetic algorithms. *Journal of The South African Institute of Mining and Metallurgy*, vol. 100, no. 2, 2000, pp. 129–134.

Banford, A.W., Aktas, Z., and Woodburn, E.T. Interpretation of the effect of froth structure on the performance of froth flotation using image analysis. *Powder Technology*, vol. 98, no. 1, 1998, pp. 61–73.

Barbian, N., Cilliers, J.J., Morar, S.H., and Bradshaw, D.J. Froth imaging, air recovery and bubble loading to describe flotation bank performance. *International Journal of Mineral Processing*, vol. 84, no. 1–4, 2007, pp. 81–88.

Cipriano, A., Guarini, M., Vidal, R., Soto, A., Sepúlveda, C., Mery, D., and Briseño, H. A real time visual sensor for supervision of flotation cells. *Minerals Engineering*, vol. 11, no. 6, 1998, pp. 489–499.

Cipriano, A., Sepulveda, C., and Guarini, M. Expert system for supervision of mineral flotation cells using artificial vision. *IEEE International Symposium on Industrial Electronics*, 1997. pp. 149–153.

Citir, C., Aktas, Z., and Berber, R. Off-line image analysis for froth flotation of coal. *Computers and Chemical Engineering*, vol. 28, no. 5, 2004, pp. 625–632.

Feng, D. and Aldrich, C. Batch flotation of a complex sulphide ore by use of pulsated sparged air. *International Journal of Mineral Processing*, vol. 60, no. 2, 2000, pp. 131–141.

Haralick, R.M., Shanmugam, K., and Dinstein, I. Textural features for image classification. *IEEE Transactions on Systems, Man and Cybernetics*, vol. 3, 1973, pp. 610–621.

Holtham, P.N. and Nguyen, K.K. On-line analysis of froth surface in coal and mineral flotation using JKFrothCam. *International Journal of Mineral Processing*, vol. 64, no. 2–3, 2002, pp. 163–180.

Kaartinen, J., Hätönen, J., Hyötyniemi, H., and Miettunen, J. Machine-vision-based control of zinc flotation—A case study. *Control Engineering Practice*, vol. 14, no. 12, 2006, pp. 1455–1466.

Kalyani, V.K., Pallavika, Chaudhuri, S., Charan, T.G., Haldar, D.D., Kamal, K.P., Badhe, Y.P., Tambe, S.S., and Kulkarni, B.D. Study of a laboratory-scale froth flotation process using artificial neural networks. *Mineral Processing and Extractive Metallurgy Review*, vol. 29, no. 2, 2008, pp. 130–142.

Moolman, D.W., Aldrich, C., Van Deventer, J.S.J., and Stange, W.W. The classification of froth structures in a copper flotation plant by means of a neural net. *International Journal of Mineral Processing*, vol. 43, no. 3–4, 1995, pp. 193–208.

Ripley, B. *Tree Structured Classifiers. Pattern Recognition and Neural Networks*. New York, Cambridge University Press, 2009. pp. 213–241.

Van Olst, M., Brown, N., Bourke, P., and Ronkainen, S. Improving flotation plant performance at Cadia by controlling and optimising the rate of froth recovery using Outokumpu FrothMaster. Australasian Institute of Mining and Metallurgy Publication Series, 2000. pp. 127–135. ◆

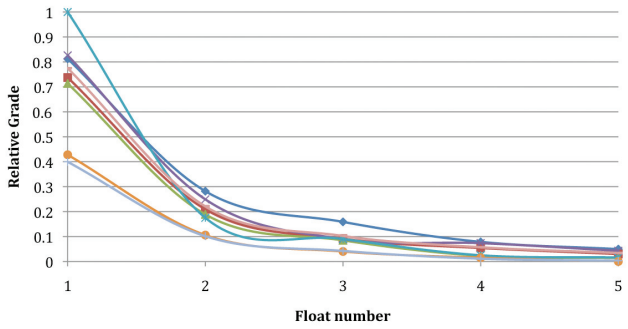

Figure 6—Assay results presented in the form of a relative grade profile

Table IV

Neural network results summary

	N - M - K	R^2 testing	Hidden layer activation function (ϕ_m)	Output layer activation function (ϕ_k)
Run 1	19-16-1	0.952	Logistic	Logistic
Run 2	19-12-1	0.917	Logistic	Logistic
Run 3	19-8-1	0.877	Tanh	Logistic
Run 4	19-17-1	0.831	Tanh	Logistic
Run 5	19-12-1	0.995	Tanh	Tanh
Run 6	19-15-1	0.990	Tanh	Identity
Run 7	19-17-1	0.989	Logistic	Logistic
Run 8	19-15-1	0.991	Tanh	Tanh
Average		0.943		